Supplement of

Elucidating the critical oligomeric steps in secondary organic aerosol and brown carbon formation

Yuemeng Ji[1,2], Qiuju Shi[1,2], Xiaohui Ma[1,2], Lei Gao[1,2], Jiaxin Wang[1,2], Yixin Li[3], Yanpeng Gao[1,2], Guiying Li[1,2], Renyi Zhang[3], and Taicheng An[1,2]

[1]Guangdong-Hong Kong-Macao Joint Laboratory for Contaminants Exposure and Health, Guangdong Key Laboratory of Environmental Catalysis and Health Risk Control, Institute Environmental Health and Pollution control, Guangdong University of Technology, Guangzhou 510006, China

[2]Guangzhou Key Laboratory of Environmental Catalysis and Pollution Control, Key Laboratory of City Cluster Environmental Safety and Green development (Department of Education), School of Environmental Science and Engineering, Guangdong University of Technology, Guangzhou 510006, China

[3]Department of Atmospheric Sciences, Texas A&M University, College Station, Texas 77843, United States

Correspondence to: Yuemeng Ji (jiym@gdut.edu.cn) and Taicheng An (antc99@gdut.edu.cn)

The choice of basis set of TSs calculation in protonation of N-containing CIs

In the oligomerization pathways of GL in the presence of MA/AM, TSs in four pathways of deprotonation from N-containing CIs were obtained. In all TSs, the TSs of the $R_{MA}612$, $R_{AM}612$, $R_{AM}653$ and $R_{AM}741$ pathways can be observed at the M06-2X/6-311G(d) and M06-2X/6-311G+(d,p) level and cannot be identified at the M06-2X/6-311G(d,p) level, while the TSs of deprotonation pathways of other N-containing CIs can be found at the M06-2X/6-311G(d,p) level. Thus, the M06-2X/6-311G(d) was used to perform the calculation instead M06-2X/6-311G(d,p) level for the $R_{MA}612$, $R_{AM}612$, $R_{AM}653$ and $R_{AM}741$ pathways.

The pointwise potential curve scanning of barrierless processes

In the method of PPC scanning, all geometric parameters were fully optimized except for the fixed internal bond length. For example, as shown in Fig. S2a, the forming O–H bond of GL protonation (GL and H^+) was successively varied from 0.7 to 3.5 Å with an interval of 0.1 Å, while other geometric parameters were fully optimized. The minimum energy occurs at the O–H distance of 1.0 Å, corresponding to the product CI11. Subsequently, the energy increases successively with the increasing O–H distance and is nearly constant when the O–H distance is about 3.0 Å, approaching the reactants. The maximum energy point corresponds to the reactants GL and H^+, rather than a TS, confirming a barrierless process of GL protonation.

Comparison of Methods

The ab initio CCSD(T) method is implemented in single-point energy calculation to assess the reliability of the M06-2X//M06-2X results. According to our previous study of the $R_{H2O}1$ pathway and Fig. S1a (Shi et al., 2020), The $\Delta G^{\ddagger}$ value of $R_{H2O}1$ at the M06-2X//M06-2X level is slightly smaller than that using the CCSD(T)//M06-2X level (44.1 kcal mol^{-1}). The ΔG_r value of $R_{H2O}1$ at the M06-2X//M06-2X level is also slightly smaller than that using the CCSD(T)//M06-2X level (3.5 kcal mol^{-1}). In addition, the ΔG_r values of the $R_{OH^-}11$ and $R_{H^+}11$ pathways are also calculated using the CCSD(T)//M06-2X level. The ΔG_r value of the $R_{OH^-}11$ pathway at the M06-2X//M06-2X level is only 3.2 kcal mol^{-1} lower than that using the CCSD(T)//M06-2X level (-10.2 kcal mol^{-1}). The ΔG_r value of the $R_{H^+}11$ pathway at the M06-2X//M06-2X level is only 1.2 kcal mol^{-1} larger than that using the CCSD(T) //M06-2X level of -98.1 kcal mol^{-1}. And water protonation provides the same ΔG_r value of -111.0 kcal mol^{-1} using two

methods. According to the above discussion, the difference of the ΔG_r values between two methods is within 4.0 kcal mol^{-1}. On the other hand, in the single-energy calculation for the same structure, the CPU time using the M06-2X method is less than that using CCSD(T) method. For example, the CPU time calculating CI11 was about 3 min on our workstation, while the CPU time was up to 259 min using CCSD(T) method. The above results indicate the M06-2X//M06-2X level presents a balance between computational accuracy and efficiency.

The calculation of rate constants

The rate constant (k) with the $\Delta G^{\ddagger}$ value was calculated using Conventional Transition State theory (TST) (Gao et al., 2014; Eyring, 1935; Evans and Polanyi, 1935; Galano and Alvarez-Idaboy, 2009) as follows:

$$k=\sigma\frac{k_B T}{h}\exp(\frac{-\Delta G^{\ddagger}}{RT}) \quad (1)$$

where k_B and h are the Boltzmann and Planck constants, respectively; $\Delta G^{\ddagger}$ is the Gibbs free energy barrier of the reaction including the thermodynamic contribution correction; σ represents the reaction path degeneracy, accounting for the number of equivalent reaction paths.

In addition, to simulate realistic conditions in the solution, the solvent cage effect is considered according to the corrections proposed by Okuno (Okuno, 1997), taking into account the free volume theory. The expression used to correct Gibbs free energy as follows:

$$\Delta G_{sol}^{FV} \backsimeq \Delta G_{sol}^{0}\text{-}RT\{\ln[n10^{(2n-2)}]\text{-}(n\text{-}1)\} \quad (2)$$

Where ΔG_{sol}^{0} is the Gibbs free energy of the reaction in the solution and n represents the molecule number of the reaction. According to expression (2), the cage effects in the solution cause the Gibbs free energy to decrease by 2.54 kcal mol^{-1} for bimolecular reactions at 298.15 K.

Some of the calculated k values were found to be close to the diffusion-limit. Thus, the apparent rate constant (k_{app}) was obtained from the effect of diffusion-limit (Collins and Kimball, 1949) besides the TST calculations:

$$k_{app}=\frac{kk_D}{k+k_D} \quad (3)$$

where the k is the thermal rate constant, obtained from TST calculations from the expression (1). k_D is the steady-state rate constant for a bimolecular diffusion-controlled reaction and is calculated as follows:

$$k_D=4\pi R D_{AB} N_A \quad (4)$$

where R denotes the reaction distance, N_A is the Avogadro number, and D_{AB} is the mutual diffusion

coefficient of the reactants A and B. D_{AB} has been calculated from D_A and D_B according to the reference (Truhlar, 1985), and D_A and D_B have been estimated from the Stokes–Einstein approach (Einstein, 1905) listed in expression (5):

$$D=\frac{k_B T}{6\pi\eta\alpha} \quad (5)$$

where k_B is the Boltzmann constant, T is the temperature, η denotes the viscosity of the solvent, which is water in our case ($\eta = 8.9 \times 10^{-4}$ Pa s), and α is the radius of the solute.

Attempt to search TSs of deprotonation from N-containing CIs initiated by H_2O

Deprotonation of N-containing CIs (N-CIs) is difficult to be initiated by H_2O, even lowering or raising the basis set. For example, we tried to optimize the intermediate ($CI_{H2O}601$) for deprotonation of $CI_{MA}601$ initiated by H_2O at the M06-2X/6-311G(d), M06-2X/6-311G(d,p), and M06-2X/6-311G+(d,p), respectively. For simplify, the geometries of $CI_{H2O}601$ at three levels denote as $CI_{H2O}601$-1, $CI_{H2O}601$-2, and $CI_{H2O}601$-3, respectively (Fig. S13). The distances of $O_{H2O}\cdots H_{N\text{-}CIs}$ and $H_{N\text{-}CIs}\cdots N_{N\text{-}CIs}$ in the $CI_{H2O}601$-2 are 1.74 and 1.04 Å, respectively, which is longer than those in $CI_{MA}601$. At the other levels, the similar results can be drawn, implying the unstable formation of $CI_{H2O}601$. In addition, using the TS keyword in geometry optimization, the TS of deprotonation of $CI_{MA}601$ by H_2O is also attempted to look for at the above levels. Three false TSs (denoted as $FTS_{H2O}601$-1, $FTS_{H2O}601$-2 and $FTS_{H2O}601$-3) are found and also presented in Fig. S13. Although only one imaginary frequency exists in three FTSs, the imaginary frequency corresponds to the instability of H_2O rather than the breaking of $H_{N\text{-}CIs}\cdots N_{N\text{-}CIs}$ and the forming of $O_{H2O}\cdots H_{N\text{-}CIs}$ bonds. Other approaches (such as HF, B3LYP, and MP2 methods) and other TSs in the similar deprotonation pathways are also attempted, and no TSs can be found. Hence, taking into account the electronegativity of N and O atoms, the deprotonation of N-CIs is difficult to be initiated by H_2O.

The description of the complexes

For each pathway of deprotonation of N-containing CIs, a complex is identified prior to the corresponding TS. The complex is consistently more stable than the corresponding reactants because of the lower ΔG_r value of the complex than that of the corresponding reactants, implying that the deprotonation of N-containing CIs proceeds via the complex and TS prior to the formation of the product. The structures of the complex are similar to those of the reactants except for the broken bonds. For

example, the structures of $COM_{MA}601$ and $COM_{AM}601$ are similar to those of $CI_{MA}601$ and $CI_{AM}601$ (Fig. S12). The broken N−H distances are elongated to 1.09 Å and 1.13 Å for $COM_{MA}601$ and $COM_{AM}601$, respectively, while other bond distances are almost consistent with corresponding reactants.

The nucleophilic addition of 1st-CB2 with MA

The multistep processes of 1st-CB2 with MA are shown as the following (Figs. S16-S17),

$$R_{MA}68\text{-}R_{MA}69:\ 1^{st}\text{-CB2} \xrightarrow{\mathbf{R_{MA}681:}\ +\ MA} CI_{MA}681 \xrightarrow{\mathbf{R_{MA}682:}\ +\ SO_4^{2-}} TS_{MA}681 \xrightarrow{-\ HSO_4^-} N\text{-}ROD_{MA}4 \xrightarrow{\mathbf{R_{MA}691}:\ +\ H^+}$$

$$CI_{MA}691 \xrightarrow{\mathbf{R_{MA}692:}\ -H_2O} CI_{MA}692 \xrightarrow{\mathbf{R_{MA}693:}\ +\ SO_4^{2-}} TS_{MA}691 \xrightarrow{-\ HSO_4^-} N\text{-}ROD_{MA}3$$

For the association pathway of 1st-CB2 with MA ($R_{MA}681$), the ΔG_r value is -38.2 kcal mol^{-1}. In $CI_{MA}681$, the length of the formed C−N bond is 1.50 Å (Fig. S12a). $CI_{MA}681$ is readily abstracted by SO_4^{2-} to yield $N\text{-}ROD_{MA}4$ ($R_{MA}682$). The $R_{MA}682$ pathway proceeds via a TS with the small $\Delta G^{\ddagger}$ of -1.4 kcal mol^{-1}. A pre-reactive complex ($COM_{MA}681$) is identified prior to the TS and the corresponding ΔG_r value is 2.0 kcal mol^{-1} lower than that of the corresponding reactants. The structure of $COM_{MA}681$ is similar to those of the reactants, except for the broken bonds. As shown in Fig. S16, protonation of $N\text{-}ROD_{MA}4$ at the hydroxyl group ($R_{MA}691$) yields $CI_{MA}691$, with the ΔG_r value of -126.6 kcal mol^{-1}. The subsequent dehydration of $CI_{MA}691$ ($R_{MA}692$) possesses the small exothermicity with the ΔG_r value of -9.6 kcal mol^{-1}, resulting in the formation of $CI_{MA}692$. Similar with the subsequent reaction of $CI_{MA}691$, deprotonation from $CI_{MA}692$ is also initiated by SO_4^{2-} ($R_{MA}693$) to form the other N-ROD ($N\text{-}ROD_{MA}3$), with the $\Delta G^{\ddagger}$ value of -5.0 kcal mol^{-1}. As discussed in the nucleophilic addition reaction of 1st-CB1 and MA, $N\text{-}ROD_{MA}3$ finally forms $N\text{-}ROT_{MA}2$, which subsequently undergoes the nucleophilic addition with 1st-CB2 to yield the N-heterocycles (Fig. S17),

$$R_{MA}70\text{-}R_{MA}71:\ N\text{-}ROT_{MA}2 \xrightarrow{\mathbf{R_{MA}701:}\ +\ 1^{st}\text{-CB2}} CI_{MA}701 \xrightarrow{\mathbf{R_{MA}702:}\ +\ TS_{anti\rightarrow syn}} CI_{MA}702 \xrightarrow{\mathbf{R_{MA}703:}\ +\ SO_4^{2-}}$$

$$TS_{MA}702 \xrightarrow{-\ HSO_4^-} N\text{-}IM_{MA}2 \xrightarrow{\mathbf{R_{MA}711:}\ +\ H^+} CI_{MA}711 \xrightarrow{\mathbf{R_{MA}712:}\ -\ H_2O} TS_{MA}711 \rightarrow N\text{-}CT_{MA}2$$

The nucleophilic addition of $N\text{-}ROT_{MA}2$ with 1st-CB2 ($R_{MA}701$) possesses the large exothermicity with the ΔG_r value of -28.1 kcal mol^{-1}, to overcome the barrier of subsequent intramolecular torsion. The intramolecular torsion from $CI_{MA}701$ to $CI_{MA}702$ proceeds via a TS, with the small $\Delta G^{\ddagger}$ value of 5.3 kcal mol^{-1}. $CI_{MA}702$ subsequently undergoes the H-abstraction to form $N\text{-}IM_{MA}2$ with a $\Delta G^{\ddagger}$ value of 30.8 kcal mol^{-1}. Protonation of $N\text{-}IM_{MA}2$ proceeds at hydroxyl groups to form $CI_{MA}711$ ($R_{MA}711$), which undergoes dehydration ($R_{MA}712$) via a TS, to yield N-containing cyclic tetramer ($N\text{-}CT_{MA}2$). The ΔG_r

value of $R_{MA}711$ is -97.3 kcal mol^{-1}, which is enough negative to favor subsequent dehydration with a small $\Delta G^{\ddagger}$ value (6.2 kcal mol^{-1}).

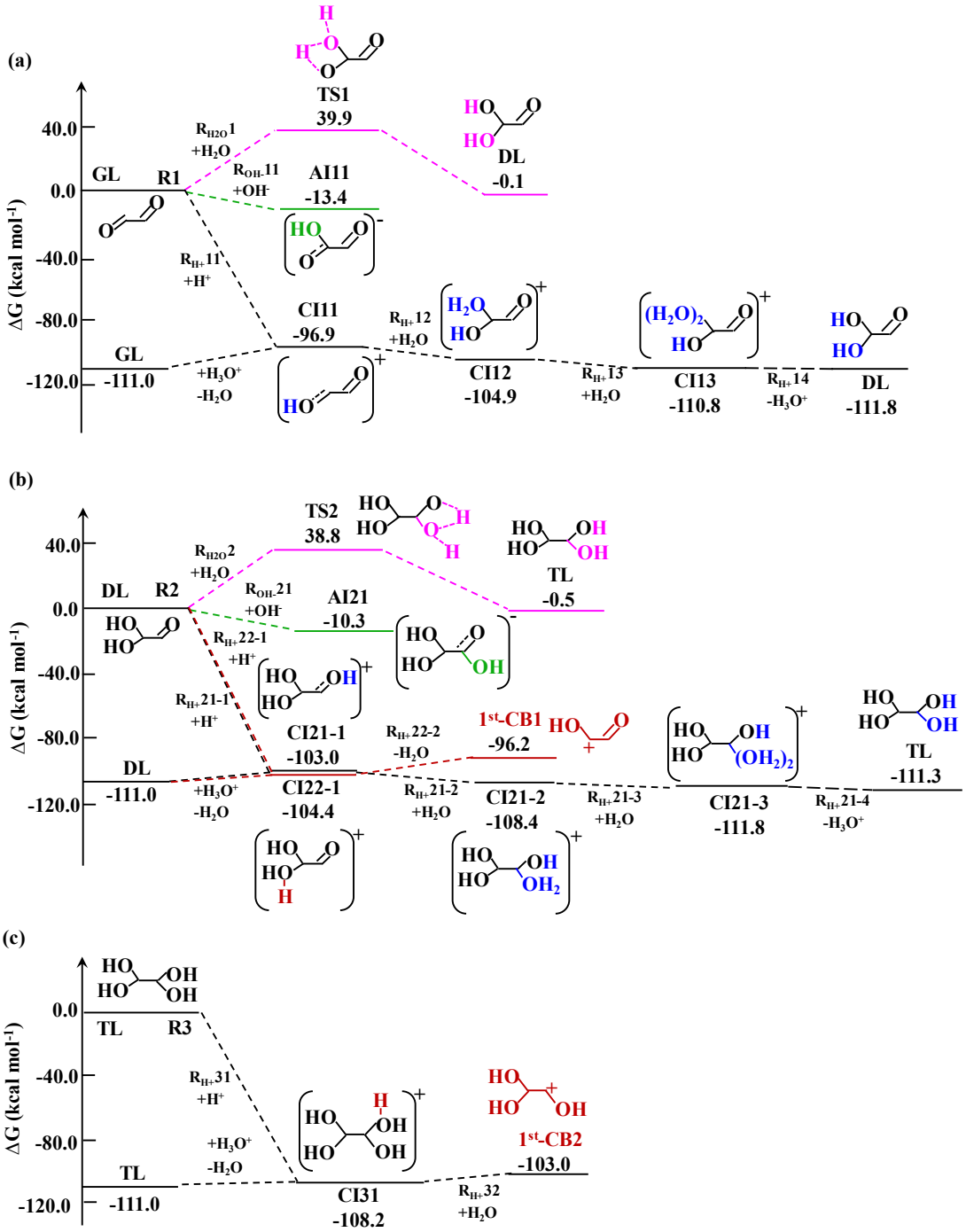

Figure S1. PESs of initial reactions of (a) GL, (b) DL and (c) TL.

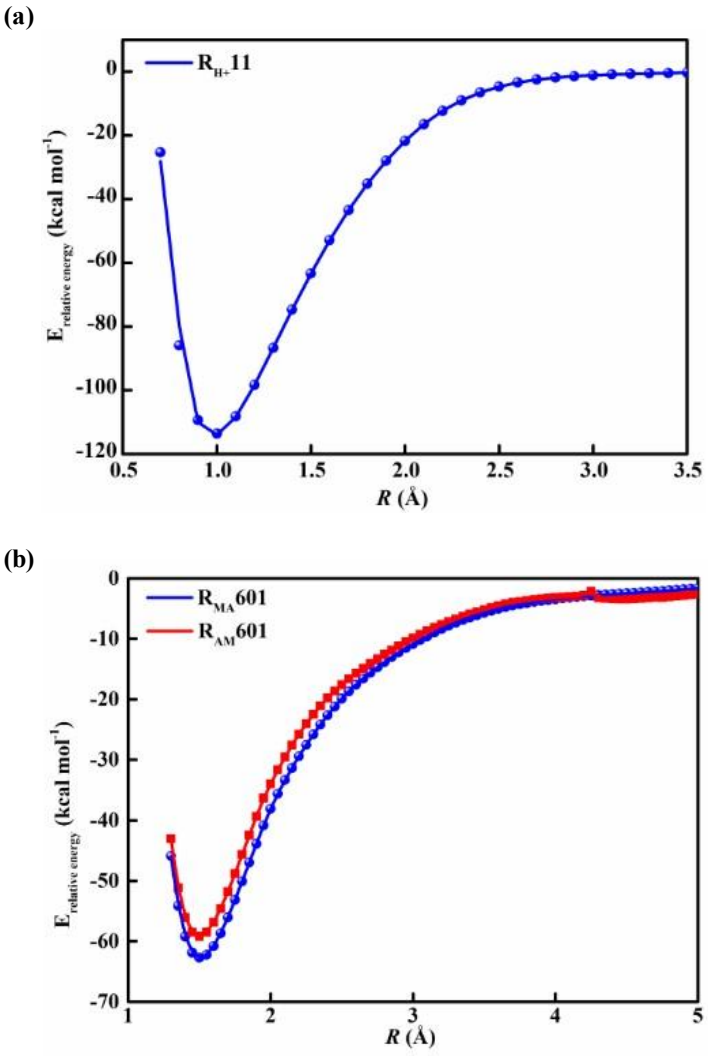

Figure S2. The potential energy curves of (a) protonation pathway of GL and (b) nucleophilic addition of 1st-CB1 with MA and AM at the M06-2X/6-311G(d,p) level. *R* represents (a) the distance of H^+ and O_{GL} atoms and (b) the distance of $N_{MA/AM}$ and $C_{1st\text{-}CB1}$ atoms, respectively.

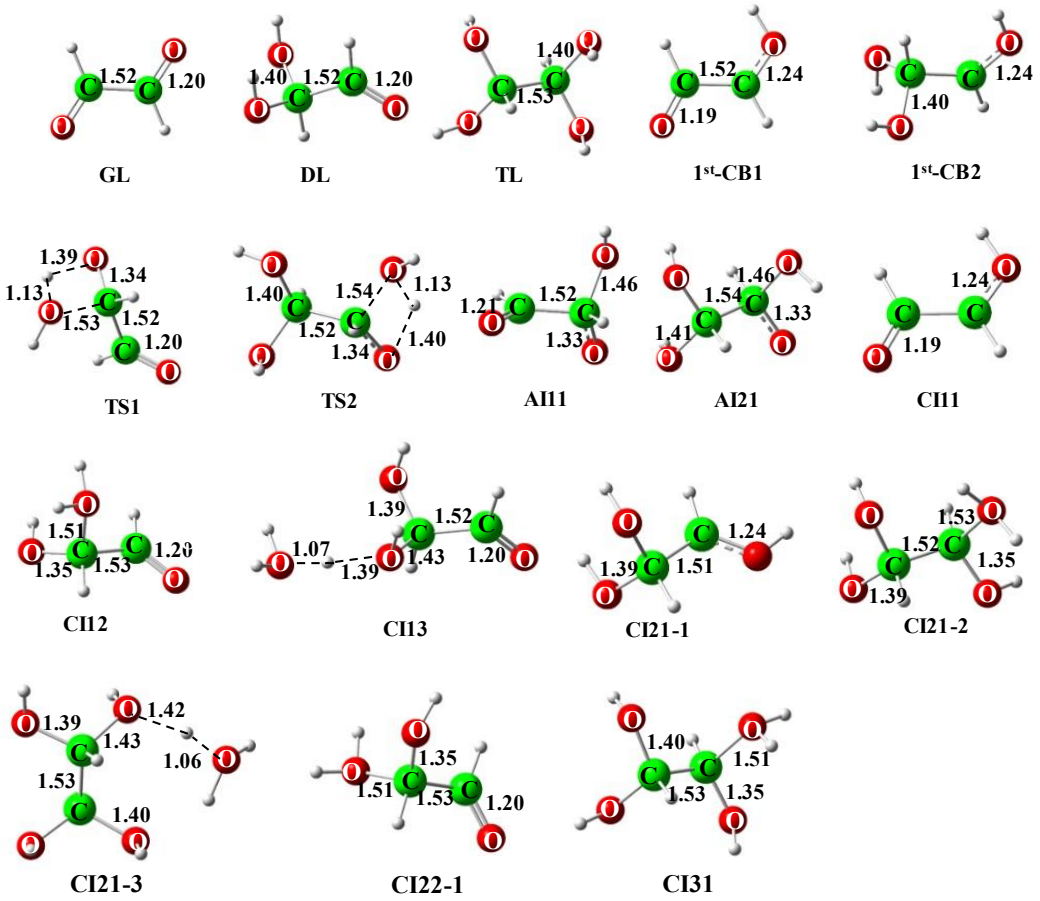

Figure S3. The optimized geometries of all SPs in the initial reactions of GL at the M06-2X/6-311G(d,p) level (in Å).

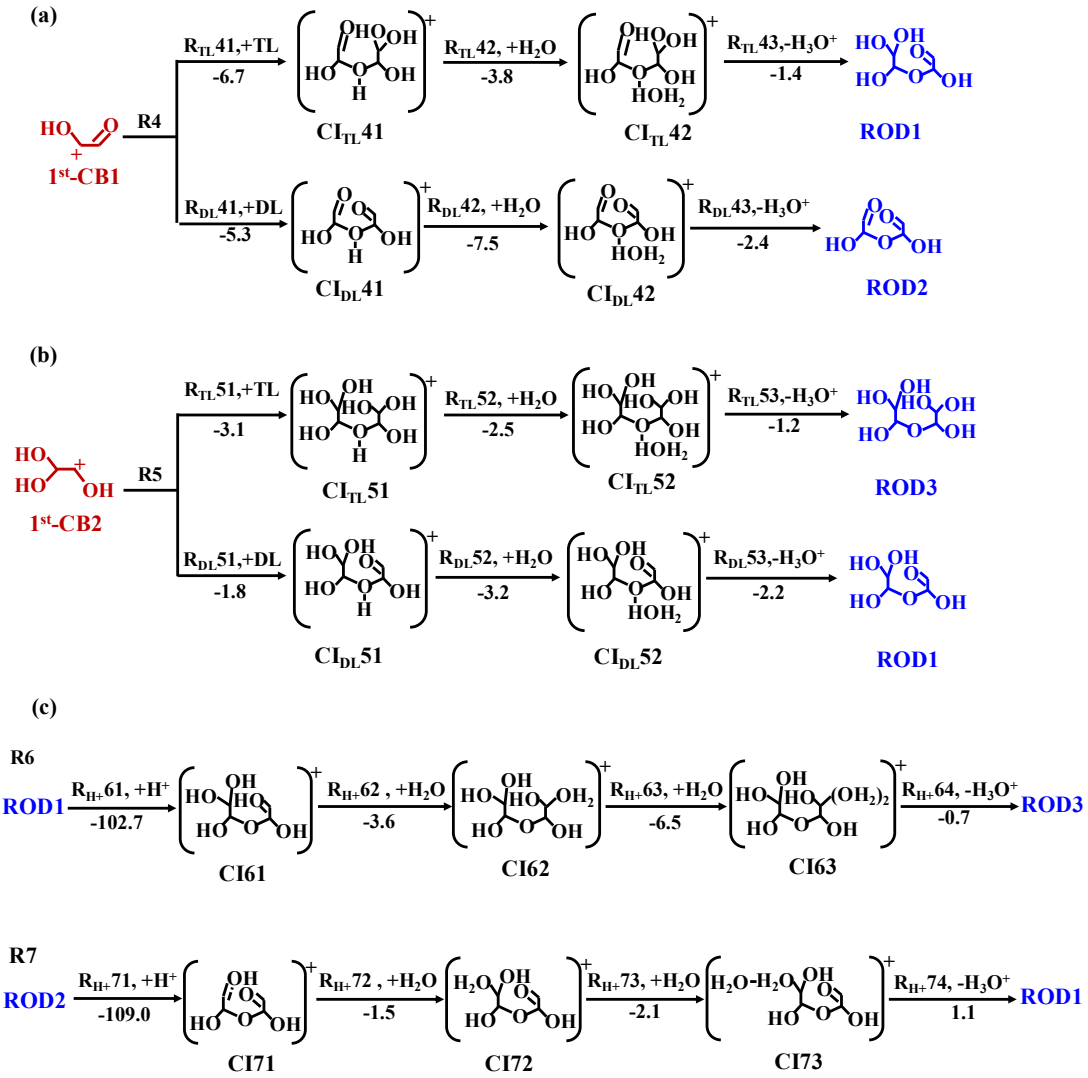

Figure S4. Self-oligomerization of GL. (a) the pathways of 1st-CB1 association with DL and TL; (b) the pathways of 1st-CB2 association with DL and TL; (c) the intermolecular isomerization pathways of RODs. The value denotes the ΔG_r of each step reaction (in kcal mol^{-1}).

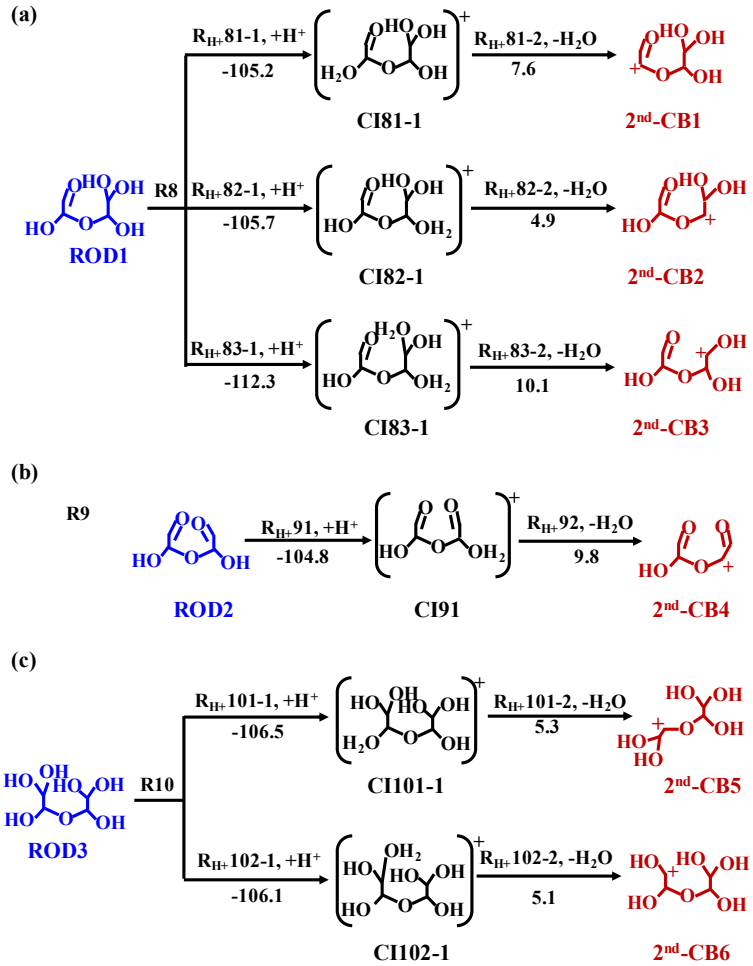

Figure S5. The formation of 2nd-CBs from (a) ROD1, (b) ROD2 and (c) ROD3. The value represents the ΔG_r of each step reaction (in kcal mol^{-1}).

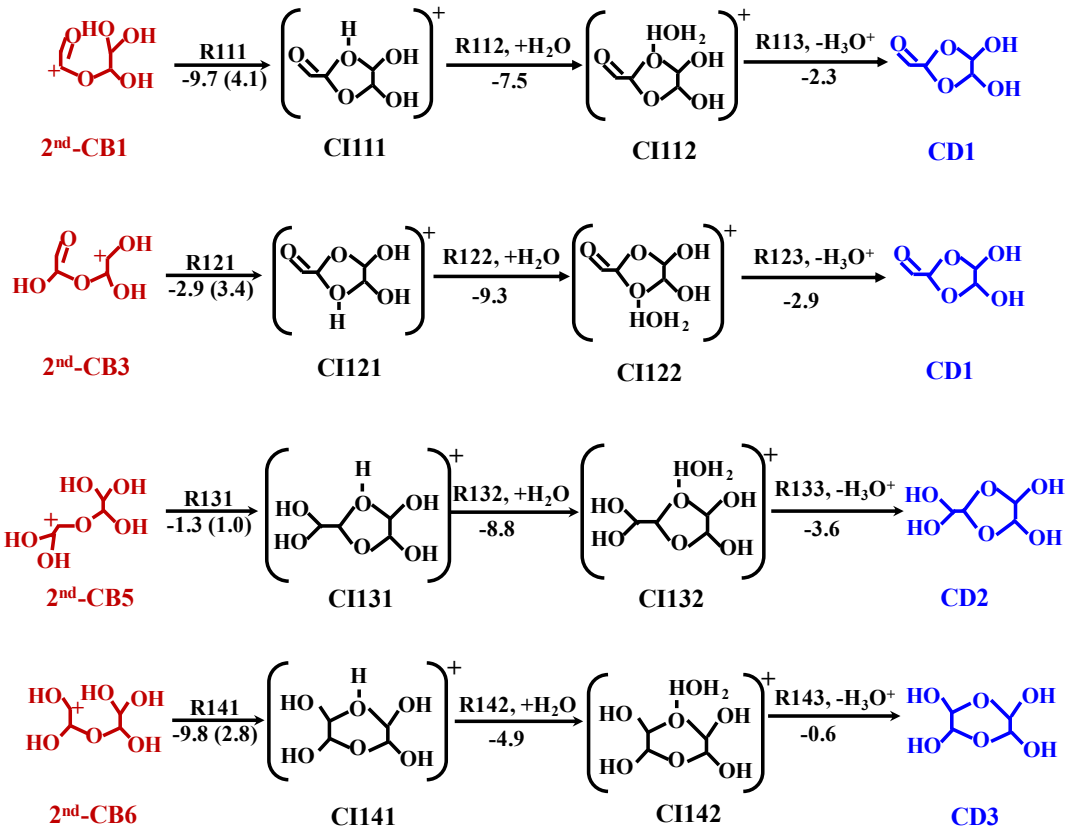

Figure S6. The pathways of 2[nd]-CBs to CDs. The value represents the ΔG_r or $\Delta G^{\ddagger}$ (in parentheses) of each step reaction (in kcal mol^{-1}).

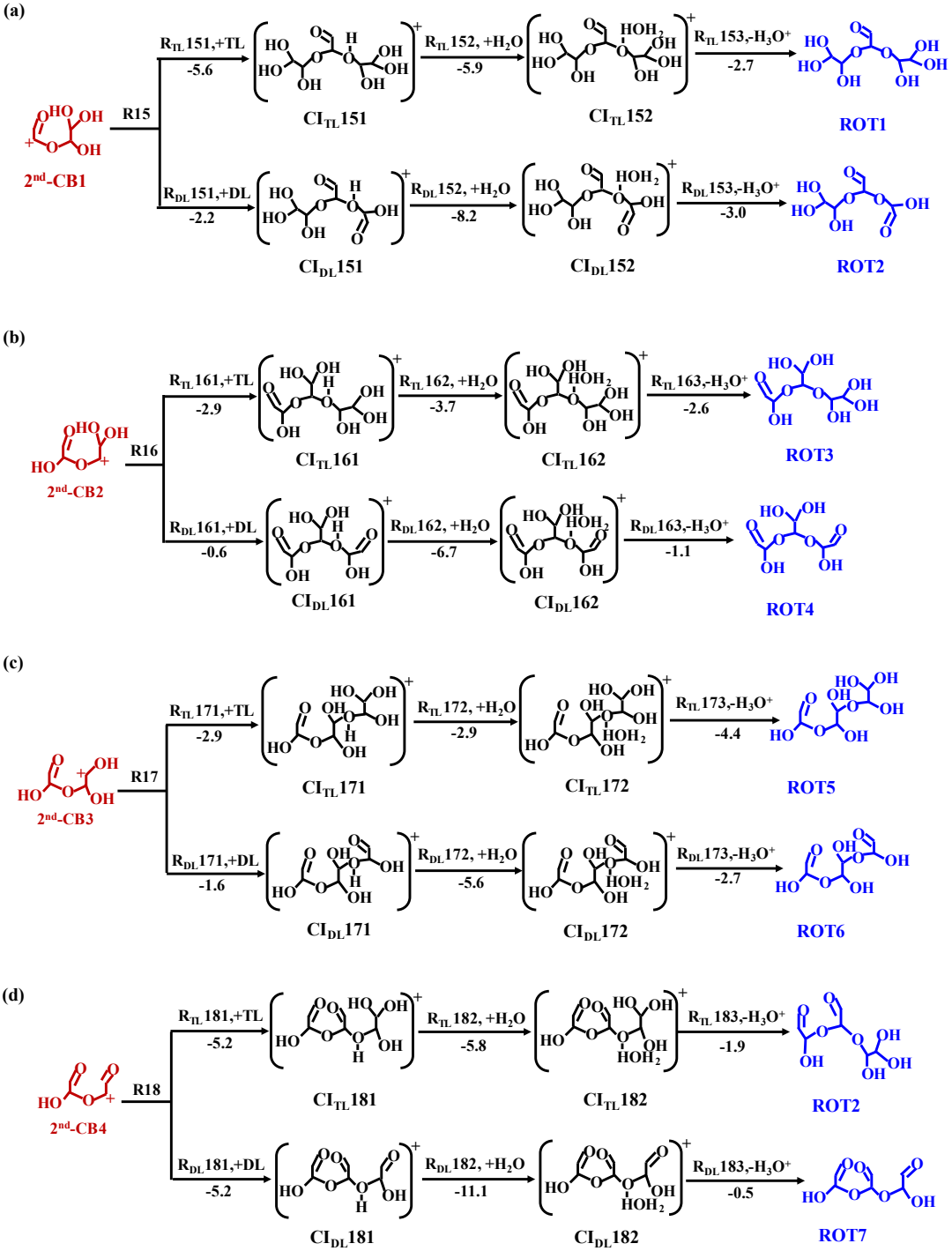

Figure S7a-d. Pathways of association reactions of DL and TL with (a) 2nd-CB1, (b) 2nd-CB2, (c) 2nd-CB3, and (d) 2nd-CB4. The value represents the ΔG_r of each step reaction (in kcal mol^{-1}).

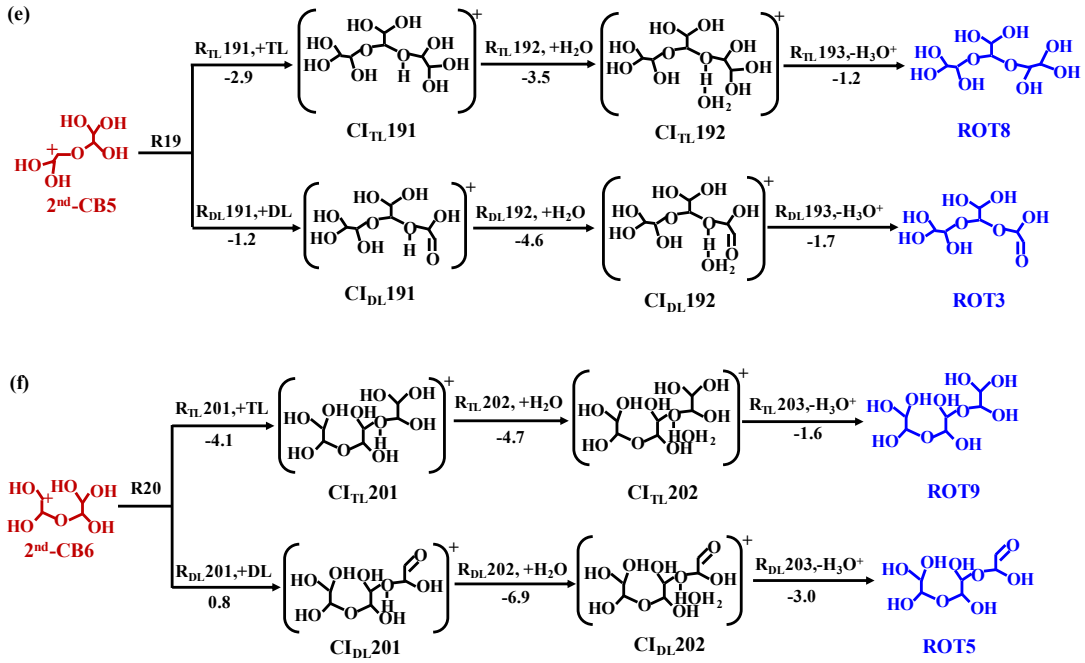

Figure S7e-f. Pathways of association reactions of DL and TL with (e) 2^{nd}-CB5, and (f) 2^{nd}-CB6. The value represents the ΔG_r of each step reaction (in kcal mol^{-1}).

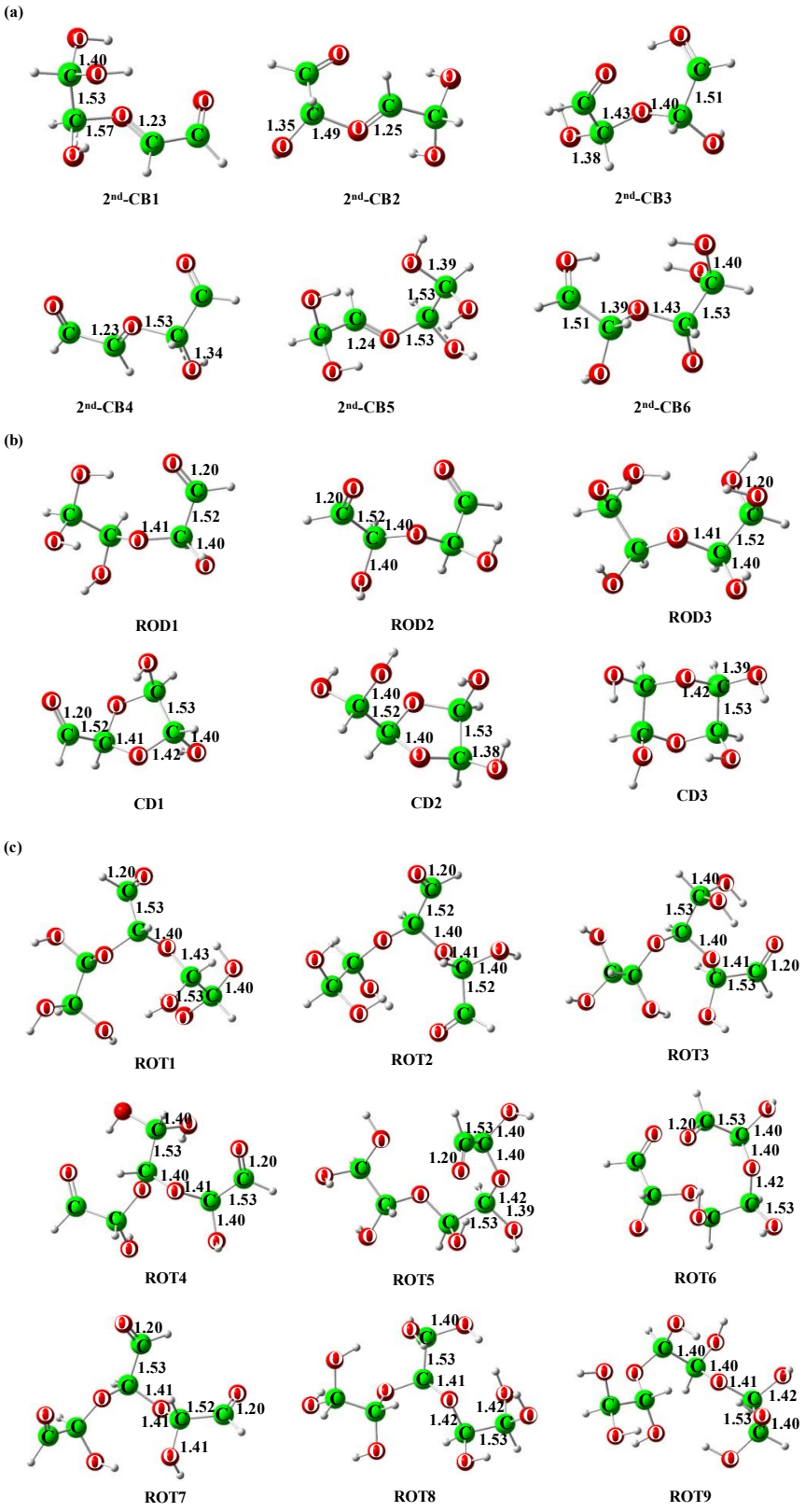

Figure S8. The optimized geometries of (a) 2nd-CBs, (b) RODs and CDs, and (c) ROTs at the M06-2X/6-311G(d,p) level. The values are the bond lengths (in Å).

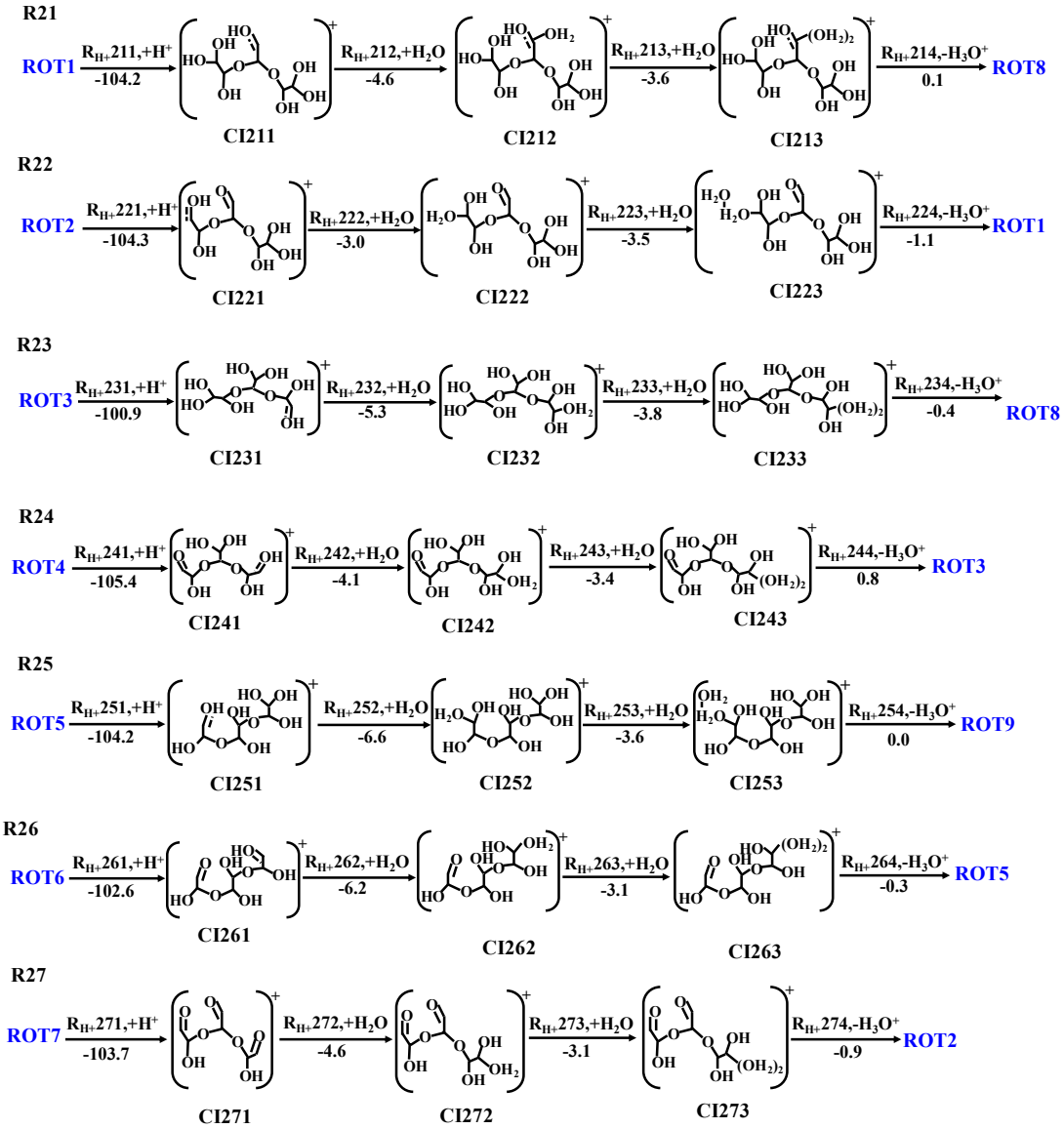

Figure S9. Pathways of intermolecular isomerization of ROTs. The value represents the ΔG_r of each step reaction (in kcal mol^{-1}).

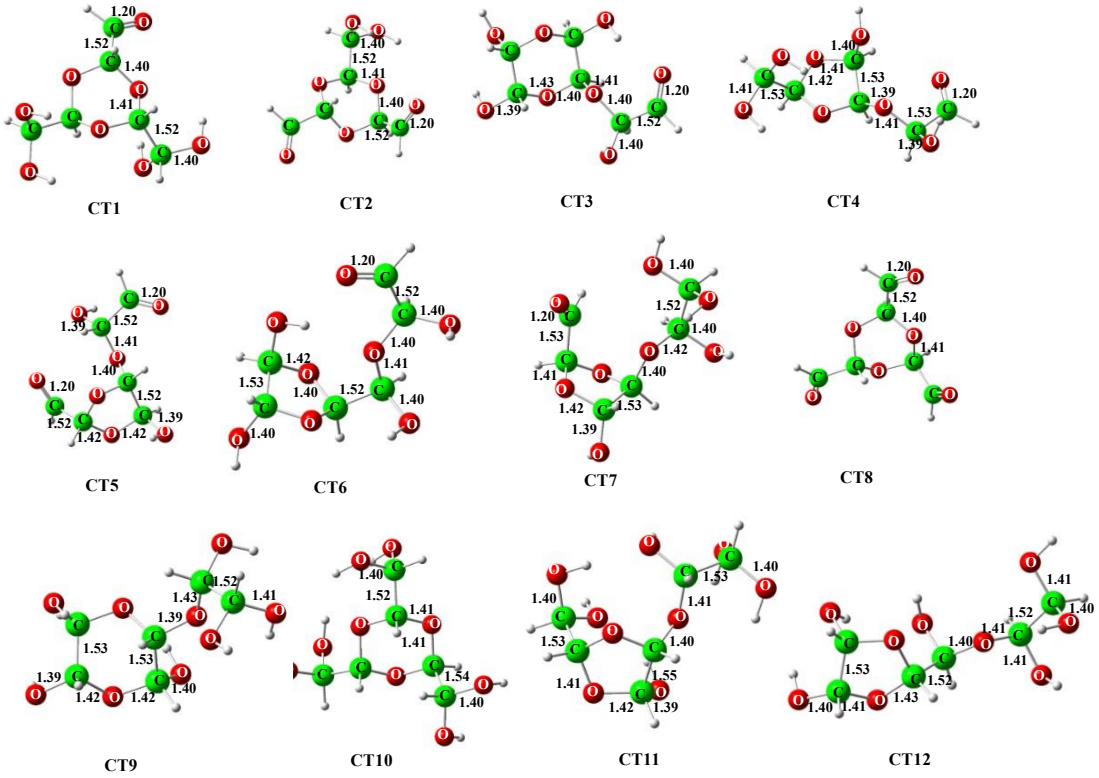

Figure S10. The optimized structures of cyclic trimers (in Å).

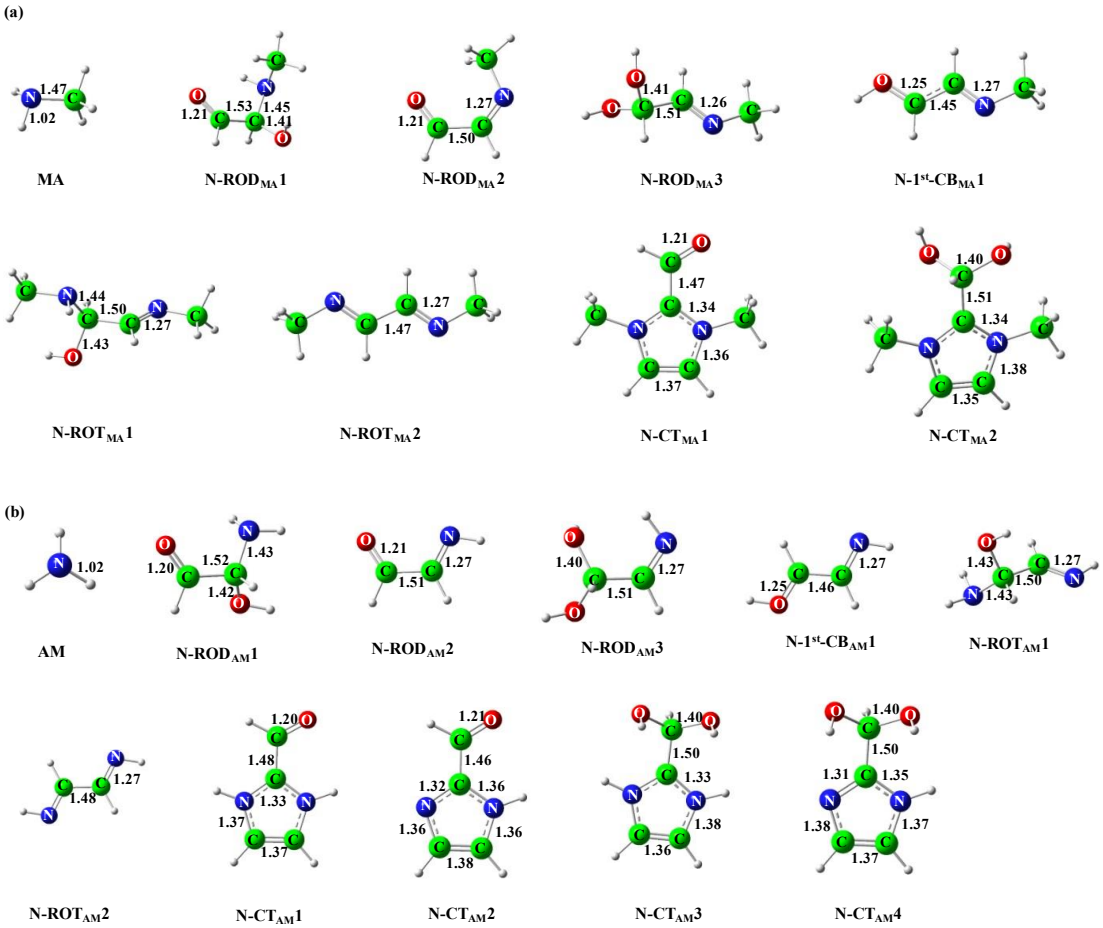

Figure S11. The optimized geometries of the SPs for the N-oligomerization (a) for MA and (b) for AM at the M06-2X/6-311G(d,p) level. The values are the bond lengths (in Å).

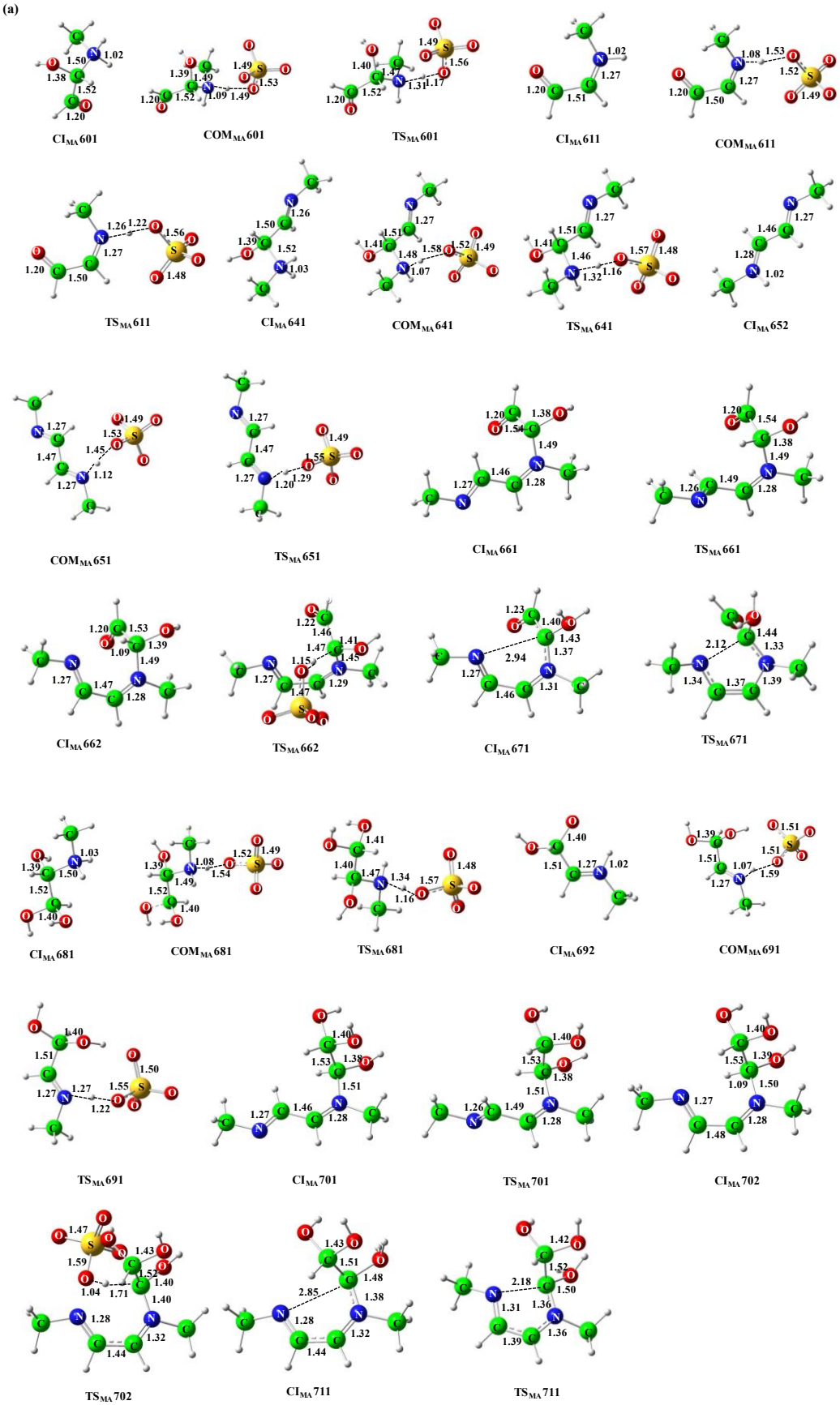

Figure S12a. The optimized geometries of the key SPs for the N-oligomerization with MA at the M06-2X/6-311G(d,p) level. The values are the bond lengths (in Å).

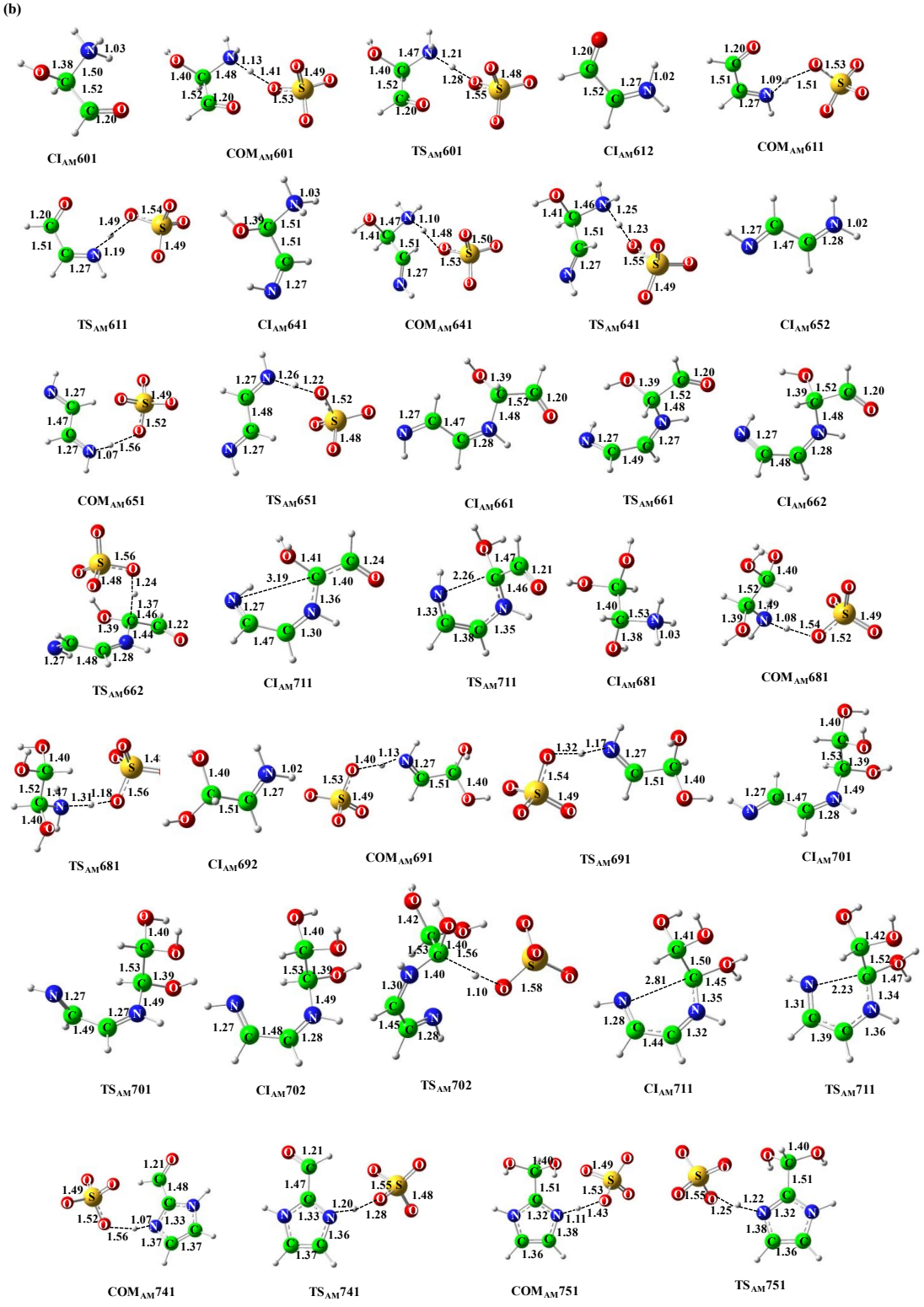

Figure S12b. The optimized geometries of the key SPs for the N-oligomerization with AM at the M06-2X/6-311G(d,p) level. The values are the bond lengths (in Å).

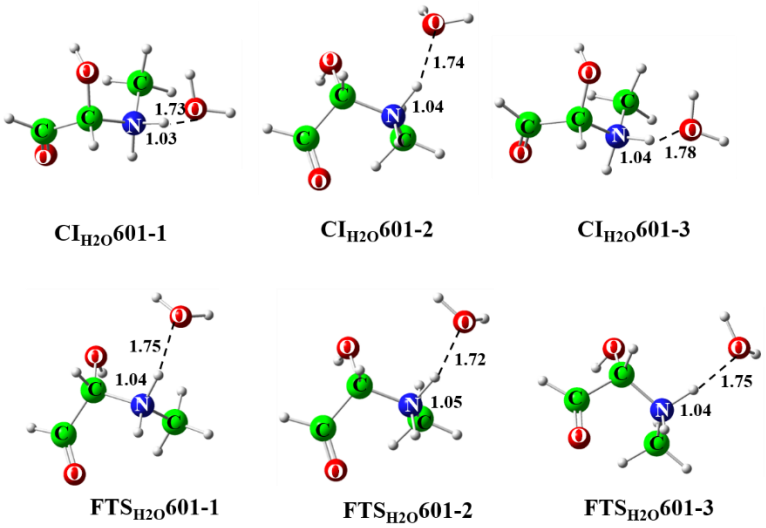

Figure S13. The optimized geometries of the deprotonation of CI$_{MA}$601 initiated by H_2O at the M06-2X/6-311G(d), M06-2X/6-311G(d,p), and M06-2X/6-311G+(d,p) levels, respectively.

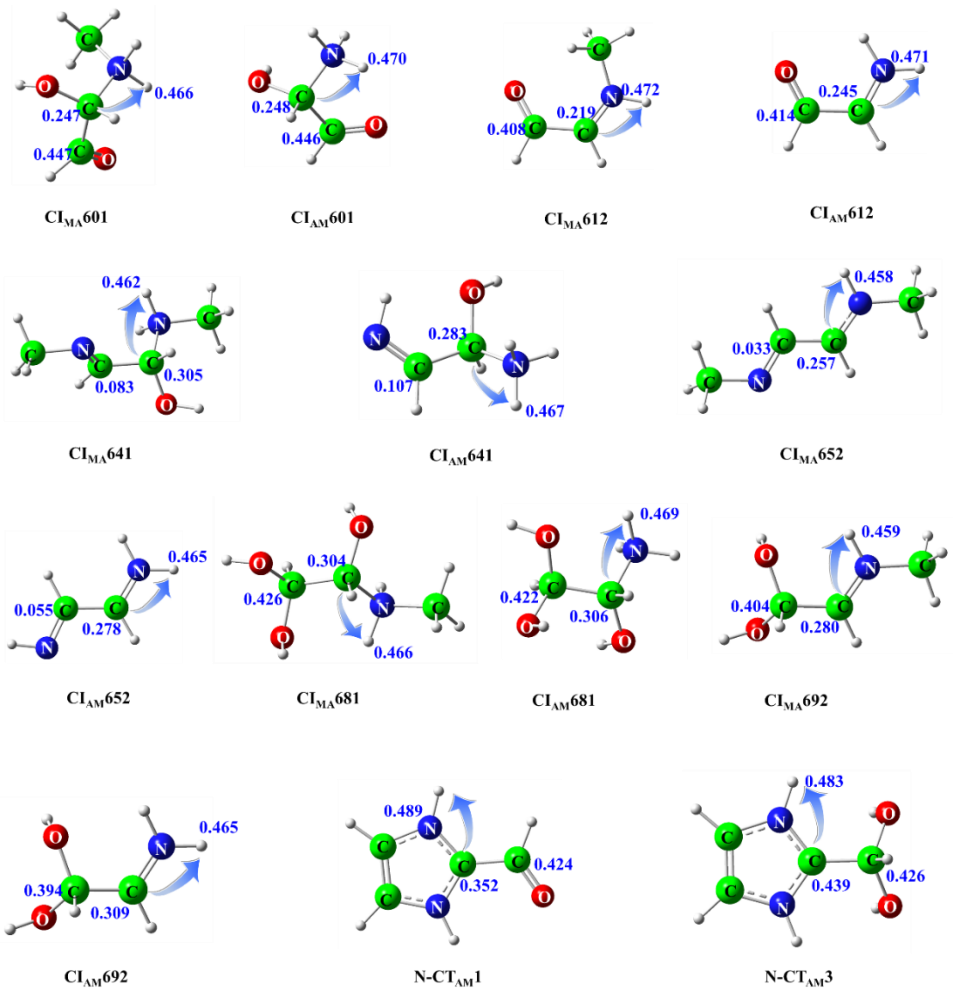

Figure S14. Schematic diagram of the positive center transfer from C-atom to H-atom in N-oligomerization (in e).

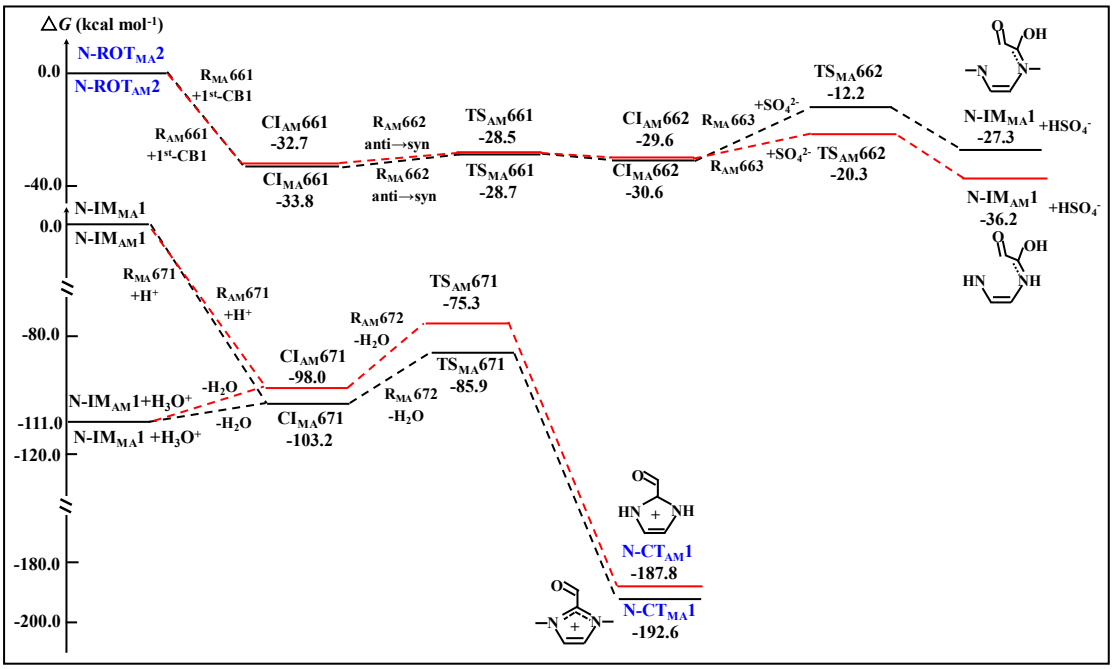

Figure S15. PESs of N-containing cyclic oligomers formation from association reactions of N-ROT$_{MA}$2/N-ROT$_{AM}$2 and 1st-CB1.

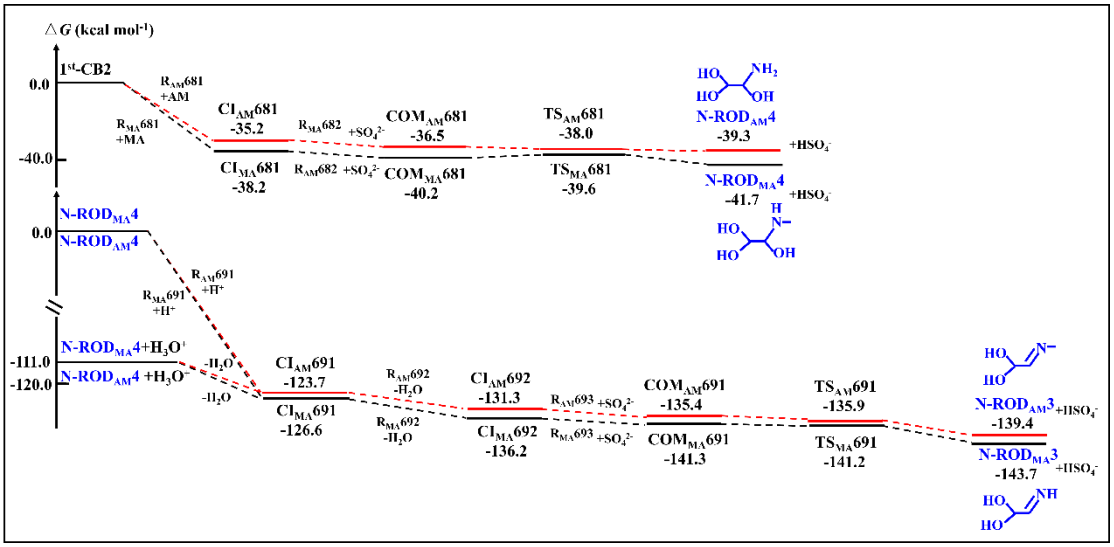

Figure S16. PESs of N-RODs formation from association reactions of 1st-CB2 with MA and AM.

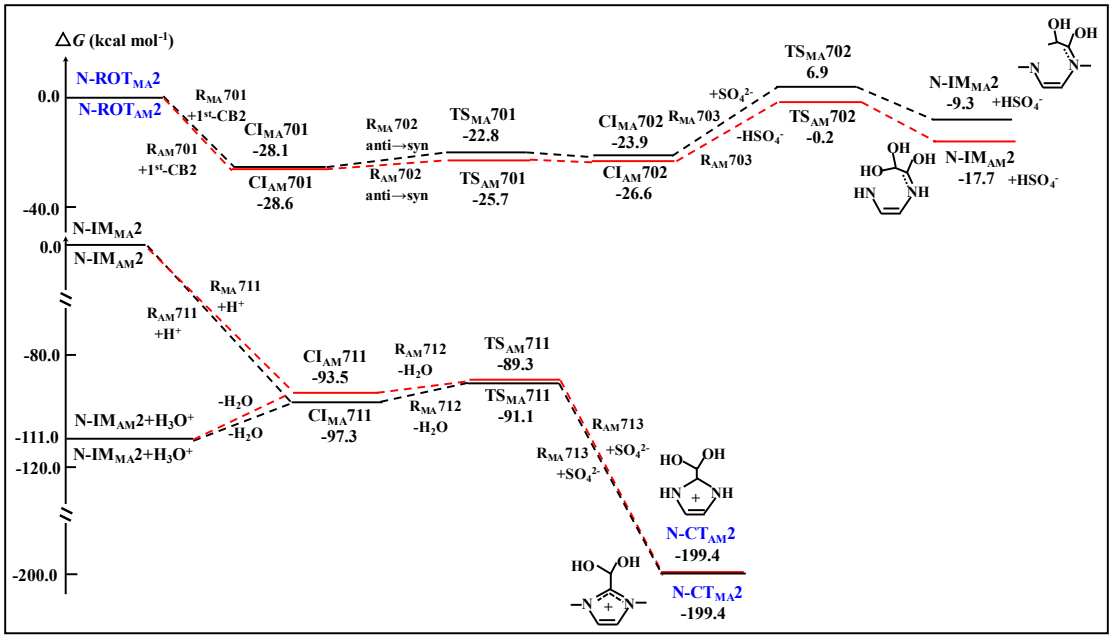

Figure S17. PESs of N-containing cyclic oligomers formation from association reaction of N-ROT$_{MA}$2/N-ROT$_{AM}$2 and 1st-CB2.

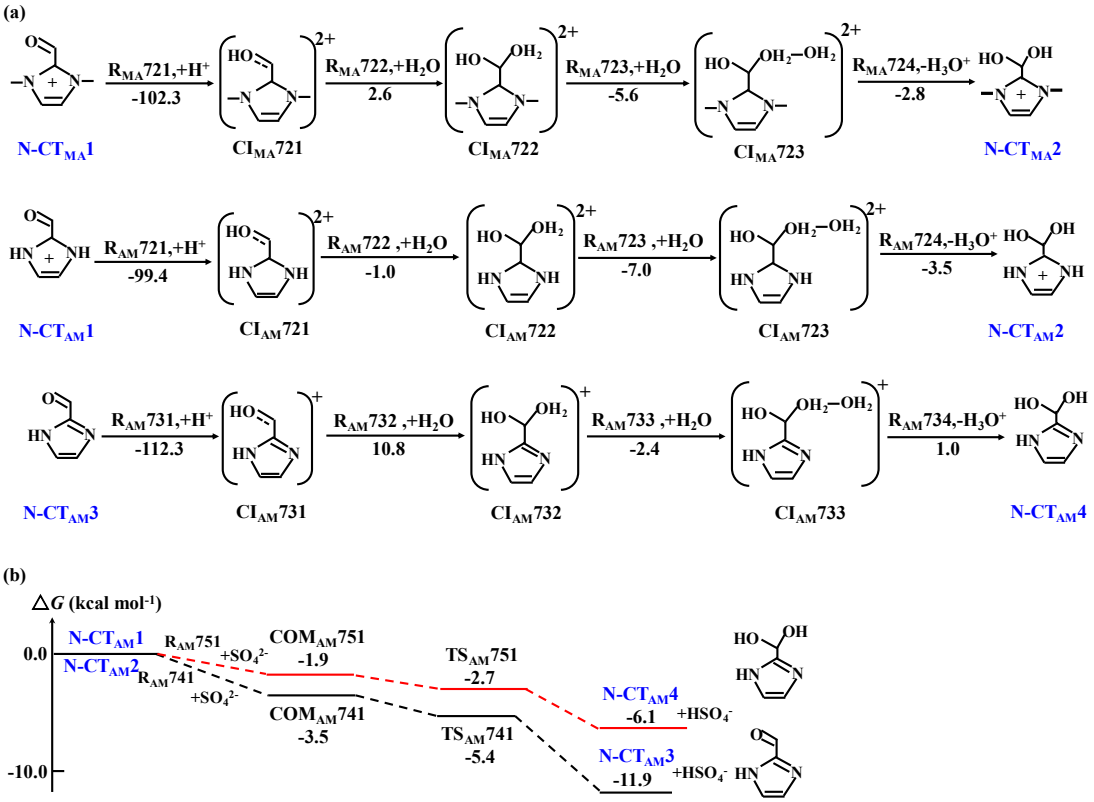

Figure S18. Subsequent conversion of N-CTs (in kcal mol^{-1}). (a) Pathways of the intermolecular isomerization of N-CTs; (b) PES of deprotonation of N-CT$_{AM}$1 and N-CT$_{AM}$2.

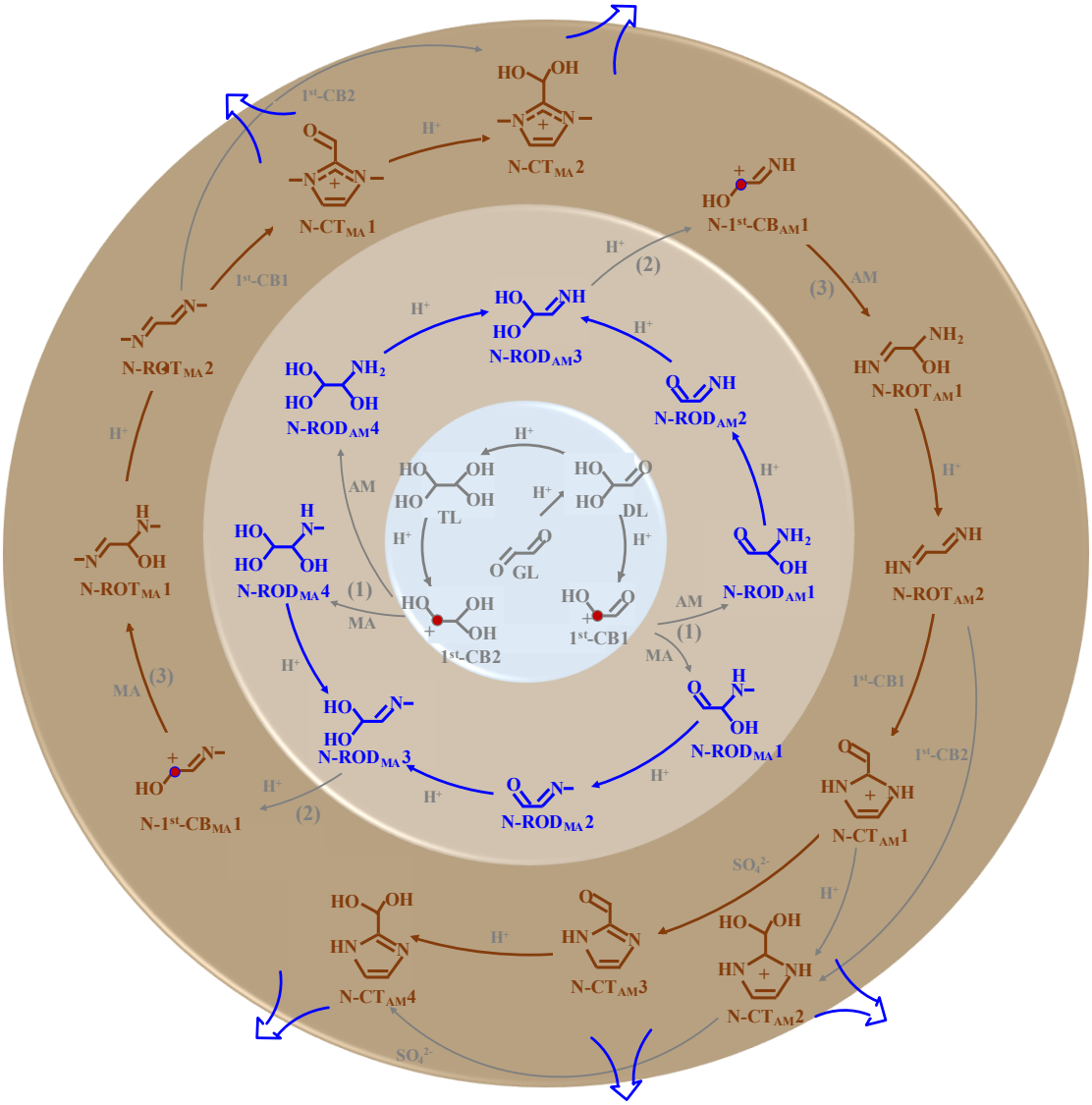

Figure S19. All possible pathways in the ion-mediated N-oligomerization of GL in the presence of MA/AM.

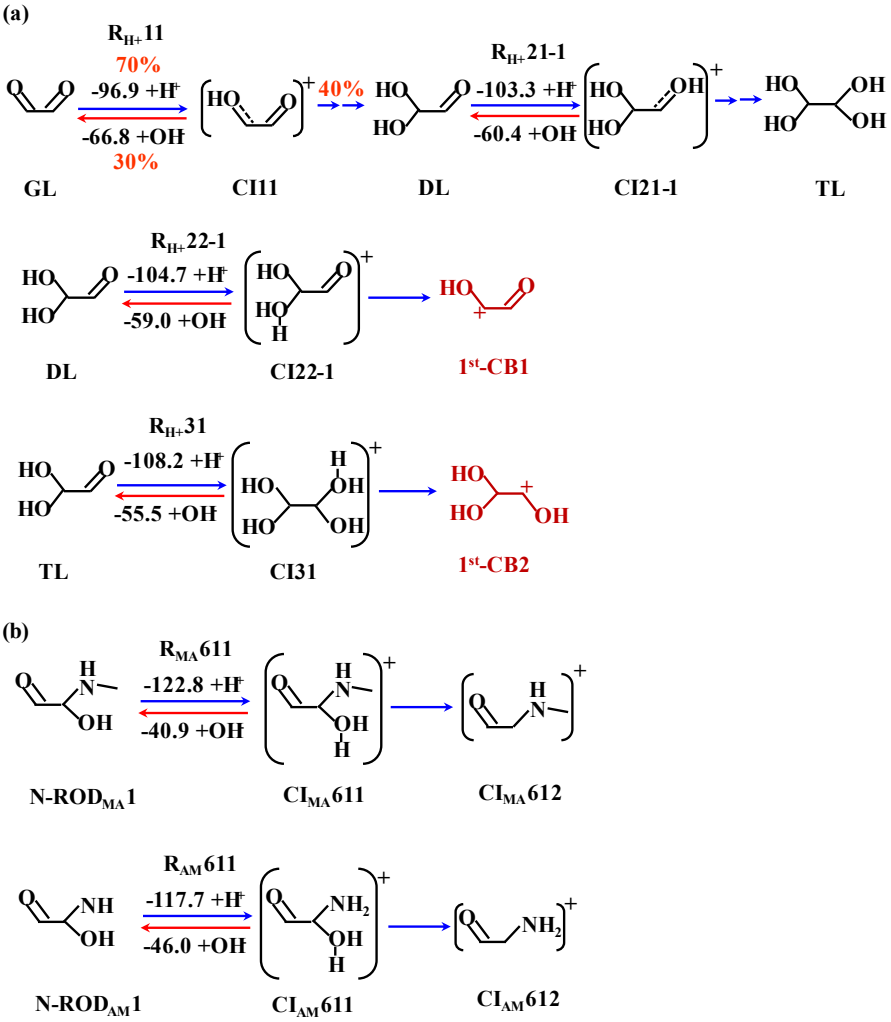

Figure S20. The competing pathways of CIs (a) in the absence of MA/AM and (b) in the presence of MA/AM (in kcal mol^{-1}). The blue color represents forward reaction by the protonation and the red color corresponds reverse reaction with OH^-.

Table S1. The activation barrier energies ($\Delta G^{\ddagger}$), the reaction energies (ΔG_r), the rate constants (k and k_{total}) and the half-lives ($t_{1/2}$) of the pathways involved the initial reaction of GL at 298 K.

Pathways	Reactions	ΔG_r / $\Delta G^{\ddagger}$ (kcal mol^{-1})	k ($\times 10^9$) (M^{-1} s^{-1})	[a]$t_{1/2}$ ($\times 10^{-4}$) (s)	k_{total} ($\times 10^9$) (M^{-1} s^{-1})
R1:					
R_{OH^-}11	GL + OH^- → AI11	-13.4	1.82	5.49	6.02
R_{H^+}11	GL + H^+ → CI11	-96.9	4.20	2.38	
R_{OH^-}12	CI11 + OH^- → GL	-66.8	1.47		3.43
R_{H^+}12	CI11 + H_2O → CI12	-7.6	1.96		
R2:					
R_{H2O}2	DL + H_2O → TL	-0.2 / 38.8	5.3×10^{-22}		
R_{OH^-}21	DL + OH^- → AI21	-10.6	1.79	5.59	10.1
R_{H^+}21-1	DL + H^+ → CI21-1	-103.3	4.14	2.42	
R_{H^+}22-1	DL + H^+ → CI22-1	-104.7	4.14	2.42	
R_{OH^-}21-1	CI21-1 + OH^- → DL	-60.4	1.50		
R_{H^+}21-2	CI21-1 + H_2O → CI22	-5.0	2.03		3.53
R_{OH^-}22-1	CI22-1 + OH^- → DL	-59.0	1.48		1.48
R3:					
R_{H^+}31	TL+H^+ → CI31	-108.2	4.13		4.13
R_{OH^-}31	CI31 + OH^- → TL	-55.5	1.65		1.65

[a]$t_{1/2}$ is given as the inverse of $[H^+] \times k$. $[H^+]$ is estimated as 10^{-6} M in weakly acidic condition.

Table S2. The reaction energies (ΔG_r) of the pathways for CTs formation at the M06-2X//M06-2X level (in kcal mol^{-1}).

Pathways	Reactions	ΔG_r
R37:		
R371	3^{rd}-CB1 → CI371	-4.2
R372	CI371 + H_2O → CI372	-5.2
R373	CI372 - H_3O^+ → CT1	-2.3
R38:		
R381	3^{rd}-CB3 → CI381	-7.1
R382	CI381 + H_2O → CI382	-10.3
R383	CI382 - H_3O^+ → CT2	0.3
R39:		
R391	3^{rd}-CB4 → CI391	-0.5
R392	CI391 + H_2O → CI392	-9.3
R393	CI392 - H_3O^+ → CT2	-2.9
R40:		
R401	3^{rd}-CB6 → CI401	-9.1
R402	CI401 + H_2O → CI402	-4.3
R403	CI402 - H_3O^+→ CT3	-1.0
R41:		
R411	3^{rd}-CB7 → CI411	-7.5
R412	CI411 + H_2O → CI412	-5.3
R413	CI412 - H_3O^+ → CT4	-1.3
R42:		
R421	3^{rd}-CB8 → CI421	1.7
R422	CI421 + H_2O → CI422	-8.3
R423	CI422 - H_3O^+ → CT1	-3.4
R43:		
R431	3^{rd}-CB9 → CI431	-12.5
R432	CI431 + H_2O → CI432	-7.1
R433	CI432 - H_3O^+ → CT1	-4.5
R44:		
R441	3^{rd}-CB10 → CI441	-0.6
R442	CI441 + H_2O → CI442	-8.7
R443	CI442 - H_3O^+ → CT2	-4.8
R45:		
R451	3^{rd}-CB11 → CI451	-3.5
R452	CI451 + H_2O → CI452	-7.4
R453	CI452 - H_3O^+ → CT5	-6.5
R46:		
R461	3^{rd}-CB12 → CI461	-7.5
R462	CI461 + H_2O → CI462	-6.2
R463	CI462 - H_3O^+ → CT6	-2.7
R47:		
R471	3^{rd}-CB13 → CI471	-5.4
R472	CI471 + H_2O → CI472	-3.9
R473	CI472 - H_3O^+ → CT4	-2.4
R48:		
R481	3^{rd}-CB14 → CI481	-0.4
R482	CI481 + H_2O → CI482	-5.4
R483	CI482 - H_3O^+ → CT7	-12.2
R49:		
R491	3^{rd}-CB15 → CI491	-4.6
R492	CI491 + H_2O → CI492	-7.1
R493	CI492 - H_3O^+ → CT4	-2.3
R50:		
R501	3^{rd}-CB16 → CI501	-6.8
R502	CI501 + H_2O → CI502	-7.4
R503	CI502 - H_3O^+ → CT7	-6.4
R51:		
R511	3^{rd}-CB17 → CI511	-4.9
R512	CI511 + H_2O → CI512	-12.2

R513	CI512 - $H_3O^+ \rightarrow$ CT5	-0.6
R52:		
R521	3^{rd}-CB18 $\rightarrow$ CI521	-5.1
R522	CI521 + $H_2O \rightarrow$ CI522	-7.7
R523	CI522 - $H_3O^+ \rightarrow$ CT5	-4.2
R53:		
R531	3^{rd}-CB19 $\rightarrow$ CI531	-5.2
R532	CI531 + $H_2O \rightarrow$ CI532	-8.5
R533	CI532 - $H_3O^+ \rightarrow$ CT8	-5.2
R54:		
R541	3^{rd}-CB20 $\rightarrow$ CI541	-7.6
R542	CI541 + $H_2O \rightarrow$ CI542	-3.3
R543	CI542 - $H_3O^+ \rightarrow$ CT9	-2.2
R55:		
R551	3^{rd}-CB21 $\rightarrow$ CI551	-7.9
R552	CI551 + $H_2O \rightarrow$ CI552	-4.1
R553	CI552 - $H_3O^+ \rightarrow$ CT10	-4.5
R56:		
R562	3^{rd}-CB22 $\rightarrow$ CI561	-10.7
R562	CI561 + $H_2O \rightarrow$ CI562	-6.1
R563	CI562 - $H_3O^+ \rightarrow$ CT11	-1.6
R57:		
R571	3^{rd}-CB23 $\rightarrow$ CI571	-1.5
R572	CI571 + $H_2O \rightarrow$ CI572	-11.7
R573	CI572 - $H_3O^+ \rightarrow$ CT11	0.3
R58:		
R581	3^{rd}-CB24 $\rightarrow$ CI581	-5.2
R582	CI581 + $H_2O \rightarrow$ CI582	-13.1
R583	CI582 - $H_3O^+ \rightarrow$ CT12	4.5
R59:		
R591	3^{rd}-CB25 $\rightarrow$ CI591	-7.3
R592	CI591 + $H_2O \rightarrow$ CI592	-8.6
R593	CI592 - $H_3O^+ \rightarrow$ CT12	-1.9

Table S3. The activation barrier energies ($\Delta G^{\ddagger}$), the reaction energy (ΔG_r), and the rate constants (k) for the pathways of protonation from N-containing CIs. Herein, the units of energies and rate constants are kcal mol^{-1} and M^{-1} s^{-1}, respectively.

Pathways	Reactions	$\Delta G^{\ddagger}$	ΔG_r	k
R_{MA}:				
$R_{MA}602$	$CI_{MA}601 + SO_4^{2-} \rightarrow N\text{-}ROD_{MA}1$	-1.7	-6.0	1.17×10^9
$R_{MA}612$	$CI_{MA}612 + SO_4^{2-} \rightarrow N\text{-}ROD_{MA}2$	-7.3	-11.6	1.27×10^9
$R_{MA}642$	$CI_{MA}641 + SO_4^{2-} \rightarrow N\text{-}ROT_{MA}1$	-1.3	-5.2	1.17×10^9
$R_{MA}653$	$CI_{MA}652 + SO_4^{2-} \rightarrow N\text{-}ROT_{MA}2$	-2.4	-7.6	1.30×10^9
$R_{MA}682$	$CI_{MA}681 + SO_4^{2-} \rightarrow N\text{-}ROD_{MA}4$	-1.4	-3.5	1.14×10^9
$R_{MA}693$	$CI_{MA}692 + SO_4^{2-} \rightarrow N\text{-}ROD_{MA}3$	-5.0	-7.5	1.30×10^9
R_{AM}:				
$R_{AM}602$	$CI_{AM}601 + SO_4^{2-} \rightarrow N\text{-}ROD_{AM}1$	-3.1	-8.2	1.32×10^9
$R_{AM}612$	$CI_{AM}612 + SO_4^{2-} \rightarrow N\text{-}ROD_{AM}2$	-5.5	-12.4	1.29×10^9
$R_{AM}642$	$CI_{AM}641 + SO_4^{2-} \rightarrow N\text{-}ROT_{AM}1$	-3.1	-7.5	1.30×10^9
$R_{AM}653$	$CI_{AM}652 + SO_4^{2-} \rightarrow N\text{-}ROT_{AM}2$	-6.1	-10.0	1.48×10^9
$R_{AM}673$	$N\text{-}CT_{AM}1 + SO_4^{2-} \rightarrow N\text{-}CT_{AM}2$	-5.5	-12.0	1.29×10^9
$R_{AM}682$	$CI_{AM}681 + SO_4^{2-} \rightarrow N\text{-}ROD_{AM}4$	-2.8	-4.1	1.22×10^9
$R_{AM}693$	$CI_{AM}692 + SO_4^{2-} \rightarrow N\text{-}ROD_{AM}3$	-4.6	-8.1	1.40×10^9
$R_{AM}713$	$N\text{-}CT_{AM}3 + SO_4^{2-} \rightarrow N\text{-}CT_{AM}4$	-2.7	-6.0	1.26×10^9

References

Collins, F. C. and Kimball, G. E.: Diffusion-controlled reaction rates, J.Colloid. Sci., 4, 425-437, doi: https://doi.org/10.1016/0095-8522(49)90023-9, 1949.

Einstein, A.: Über die von der molekularkinetischen Theorie der Wärme geforderte Bewegung von in ruhenden Flüssigkeiten suspendierten Teilchen, Ann. Phys. (Berlin), 322, 549-560, https://doi.org/10.1002/andp.19053220806, 1905.

Evans, M. G. and Polanyi, M. G.: Some applications of the transition state method to the calculation of reaction velocities, especially in solution, Trans. Fara. Soc., 31, 1965-1967, https://doi.org/10.1039/tf9353100875, 1935.

Eyring, H.: The activated complex in chemical reactions, J. Chem. Phys., 3, 107-115, https://doi.org/10.1063/1.1749604, 1935.

Galano, A. and Alvarez-Idaboy, J. R.: "Guanosine + OH radical reaction in aqueous solution: A reinterpretation of the UV-vis data based on thermodynamic and kinetic calculations", Org. Lett., 11, 5114-5117, https://doi.org/10.1021/ol901862h, 2009.

Gao, Y., Ji, Y., Li, G., and An, T.: Mechanism, kinetics and toxicity assessment of OH-initiated transformation of triclosan in aquatic environments, Water Res, 49, 360-370, https://doi.org/10.1016/j.watres.2013.10.027, 2014.

Okuno, Y.: Theoretical investigation of the mechanism of the baeyer-villiger reaction in nonpolar solvents, Chem. - Eur. J., 3, 210-218, https://doi.org/10.1002/chem.19970030208, 1997.

Shi, Q., Zhang, W., Ji, Y., Wang, J., Qin, D., Chen, J., Gao, Y., Li, G., and An, T.: Enhanced uptake of glyoxal at the acidic nanoparticle interface: implications for secondary organic aerosol formation, Environ. Sci.: Nano, 7, 1126-1135, https://doi.org/10.1039/d0en00016g, 2020.

Truhlar, D. G.: Nearly encounter-controlled reactions: the equivalence of the steady-state and diffusional viewpoints, J. Chem. Educ., 62, 104-106, https://doi.org/10.1021/ed062p104, 1985.